Melt Drawability of Ultrahigh Molecular Weight Polyethylene

Hiroki Uehara,† Mitsuhiro Nakae, and Tetsuo Kanamoto*

Department of Applied Chemistry, Science University of Tokyo, Kagurazaka, Shinjuku-ku, Tokyo 162, Japan

Anagnostis E. Zachariades

POLTECO. Inc., P.O.Box 2055, Burlingame, California 94011-2055

Roger S. Porter

Polymer Science & Engineering Department, University of Massachusetts, Amherst, Massachusetts 01003

Received September 21, 1998; Revised Manuscript Received January 20, 1999

ABSTRACT: Some ultrahigh molecular weight polyethylenes have been shown to be highly ductile but only under specific conditions. When the initial starting state is reactor powder, the ductility is presumed to be due to the low initial entanglement. Samples were prepared for such draw by compression molding of reactor powder that had been held at different temperatures in the melt for only brief periods (5 min), followed by cooling to room temperature. These films were then quickly heated and drawn at a constant temperature of 140−155 °C, above the static melting temperature ($T_m \approx 135$ °C). The stress/strain behavior from this state was found to be significantly influenced by both the prior melt temperature and the time needed for preparation of the initial morphologies. X-ray diffraction showed that the strain-induced crystallization from the melt had occurred during draw above a critical strain, corresponding to the draw ratio of ∼10. Differential scanning calorimetric data clarified that the rate of this crystallization is accelerated by the higher draw stress for the samples prepared at the higher prior-melt temperature. Combination of X-ray and calorimetric results also indicated that the samples drawn from the melt contain two kinds of crystals, i.e., highly chain-extended and oriented crystals having a higher T_m and chain-folded ones having a lower T_m. With increasing draw ratio, the relative amount of the former crystals, formed on draw, gradually increased. The efficiency of draw, evaluated from tensile tests and thermal shrinkage measurements, was also interpreted from the differences of the prior-melt conditions, which increase entanglement. The samples could be successfully drawn from melt up to a maximum draw ratio of 45−50 at the optimum temperature of 150 °C. Such highly drawn films exhibited a tensile modulus of 55 and a strength of 0.95 GPa, respectively. For the solid-state drawing below T_m, the stress/strain behavior of the samples molded at different temperatures were all identical and had a low draw ratio of ∼6. This suggests a difference in entanglements as they affect draw above and below the static melting temperature.

Introduction

Over the last 25 years, the development of mechanical properties of ultrahigh molecular weight polyethylene (UHMWPE) has been achieved by a range of ultradrawing techniques.[1−6] In 1970s, the fibrillar surface-grown crystal was obtained by solution-crystallization under shear flow by Zwijnenburg and Pennings.[1] Smith and Lemstra[2,3] successfully introduced a new technique of gel film drawing and the gel spinning methods. Gels prepared from a solution with a higher polymer concentration have a higher chain entanglement density.[7] The draw stress and drawability of such gels significantly depends on their entanglement density.

Independently, we[4] have superdrawn UHMWPE single-crystal mats, which were precipitated from dilute solution, up to a maximum draw ratio of 250. This has been accomplished by two-stage draw,[5] using first solid-state coextrusion,[6] followed by tensile drawing at controlled temperatures and rates. Such a highly drawn film exhibits a tensile modulus of 220 GPa. This value approaches the chain-axis crystal modulus of PE determined by X-ray diffraction (240 GPa).[8]

It was also found that compacted powder films of UHMWPE, compression molded below the T_m, could also be ultradrawn by using this two-stage drawing method.[9] Such highly drawn powder films achieved resultant tensile properties comparable to those of gel-process fibers and tapes. Poly(tetrafluoroethylene) powder could also be ultradrawable by this reactor powder drawing technique.[10,11] Independently, Smith et al.[12,13] have shown that UHMWPE virgin films and powders prepared by use of a low-activity catalyst exhibit high ductility. The drawability and the resultant tensile properties of drawn products were significantly affected by the polymerization conditions.[12−15] Thus, high deformability of reactor powders has been ascribed to the lower entanglement density in their virgin morphology.[16−18] Once the powders were melted, the high tensile ductility was previously thought to be lost.

Many viscoelastic and spectroscopic measurements have been made on melt and crystalline polymers of conventional $M_w < 10^6$. However, only a few reports[19,20] have been published on the properties of UHMWPE melts, mostly because of their much higher melt viscosity. It has been shown that viscoelasticity of a UHMWPE melt is independent of history once the sample has been heated into a melt, even for a short period (<∼3 min).[20] The stress/strain curve below the T_m of a

* To whom correspondence should be addressed.
† Present address: Department of Chemistry, Gunma University, Kiryu, Gunma 376-8515.

10.1021/ma981491z CCC: $18.00
Published on Web 03/19/1999

sample solution-crystallized, followed by annealing in the melt, even for a short time of 10 s, was found to be identical to that of a film directly melt-crystallized from powder.[21] These facts infer that the drawing behavior from a melt of UHMWPE would not be affected by the prior thermal history.

Recently, we[22] have reported that some reactor powders can be effectively tensile drawn, even above their static T_m. The static T_m is the melting temperature measured without any external stress. Time-resolved X-ray measurements, during such high-temperature deformation at 150−160 °C, showed that usual orthorhombic crystals transform into hexagonal ones at an early stage of draw. These oriented crystals reverse into an orthorhombic structure with increasing strain. Even at the higher drawing temperature of 160 °C, draw proceeded with development of a semicrystalline state.

In this work, we have systematically improved the method of drawing UHMWPE from the melt. The effect of prior thermal histories of samples has been studied. The influences of draw temperature and rate were also studied. It should be noted that this method involves no solvent treatment. Most other drawing techniques of UHMWPE have been tried below T_m. In contrast, the drawing process discussed in this present paper focuses on the deformation from an amorphous melt PE. This different concept allows us to expect quite different deformation behavior and structure development during draw, compared to that of the usual crystalline-state deformation. Especially, the stress/strain behavior was evaluated to estimate the entanglement formation in the prior melt.[23−27]

Experimental Section

Sample Preparation. The UHMWPE used was Hizex Million 340M from Mitsui Petrochemical. It had a viscosity-average molecular weight, M_v, of 3.3×10^6. To stabilize the reactor powder, it was soaked in acetone with a small amount of an antioxidant, 3-(3,5-di-*tert*-butyl-4-hydroxy) phenyl propanate (0.5 wt %, based on polymer), for 1 day at room temperature (RT), followed by ambient evaporation of acetone to provide an homogeneous distribution of the antioxidant within powder samples. Melt-grown crystal (MGC) films, 0.2 mm thick, were prepared by compression molding of this reactor powder, containing antioxidant at T_p (pressed temperature) = 160−230 °C and 2.5 MPa for 5 min, followed by slow cooling to RT.

Some MGC films prepared at 200 °C were also melt−annealed in a silicone oil bath kept at 200 °C for 30 min to 250 h. After this annealing, the samples were also compressed into uniform films and slowly cooled to RT. The residual silicone oil in these melt−annealed MGC films was removed over 3 h by acetone Soxhlet extraction at its boiling point.

For comparison, less-entangled solution-grown crystals (SGC) were isothermally precipitated from a dilute *p*-xylene solution of UHMWPE with 0.1 wt % (based on solvent) antioxidant. Preparation details have been described elsewhere.[5]

Drawing. The sample films were cut into strips, 7−30 × 2 × 0.2 mm^3. These ribbons were tensile drawn in an air oven equipped with a Tensilon tensile tester HTM-100. Draw was made at constant temperatures (T_d) from RT to 160 °C and at cross-head speeds corresponding to the initial strain rates ($\dot{\gamma}$) of 1−20 min^{-1}. Before drawing, the sample was kept at a given T_d for 5 min in an oven. The draw ratio (DR) was determined from the separation of ink marks preprinted on the surface of samples. The relationship between draw strain on the stress/strain curves and resultant DR is as follows:

$$\mathrm{DR} = \frac{\%\ \mathrm{strain}}{100} + 1$$

Measurements. A Seiko DSC-10 and -220 were used for differential scanning calorimetry (DSC) measurements. The heating scan was observed up to 180 °C at a heating rate (*H. R.*) of 3 °C/min under a nitrogen gas flow. Sample melting was evaluated by the peak T_m ($T_{m,peak}$). The heat of fusion (ΔH_f) and $T_{m,peak}$ were calibrated by an indium standard. Crystallinities were calculated from ΔH_f, assuming the ΔH_f of perfect PE crystals is equal to 290 J/g.[28] To avoid a constrained state of the sample induced by thermal shrinkage and delay of the heat transfer during heating scan, a small amount of silicone oil was added between the sample and the bottom of the DSC pan. It had been confirmed that the DSC baseline was stable even with silicone oil. Densities of samples were determined at 30 °C in a density gradient column consisting of the mixtures of methylcarbitol and 2-propanol. Wide-angle X-ray diffraction (WAXD) patterns were recorded on a Rigaku flat-plate camera with the incident beam perpendicular to the wide surface of the films. The Ni-filtered Cu $K\alpha$ radiation used was generated by a Rigaku type RAD-III-A X-ray generator at 40 kV and 25 mA. The thermal shrinkage tests also were made by holding samples in a hot silicone oil bath for 15 s at 220 °C. The elastic recovery, R (in percentage) was calculated from the sample lengths measured before (L_t) and after shrinkage (L_s), according to the following equation:[25]

$$R = (L_t - L_s)/(L_t - L_o) \times 100\%$$

where L_o is the sample length prior to drawing.

Results

In our previous work,[5] the tensile drawing of UHMWPE in a solid state was found to be significantly affected by several factors, including the initial morphology of the sample and drawing temperature, T_d. Such effects on the tensile stress/strain curve could be observed even on drawing above the static T_m of the sample. Further, the mats of SGC, which initially have a low chain-entanglement density were also drawn, and their drawing behavior was compared to that of the MGC films, prepared at various T_p's above T_m. The resultant tensile properties of these samples drawn from the melt were also measured. Structural changes during drawing were evaluated by X-ray, DSC, and thermal shrinkage tests.

Drawability of Reactor Powder. The drawability of the reactor powder used in this work was examined and compared with that of MGC films from the same powder, as described below. The reactor powder was compression-molded at 130 °C (below T_m). Different drawing techniques were applied for drawing of these brittle films in the solid-state below T_m. The coextrusion method led to a maximum DR (DR_{max}) of 15. Two-stage drawing techniques, first coextrusion and subsequent tensile draw, gave a $DR_{max} \approx 10$. However, they were also significantly higher than the solid-state drawability of the MGC films of this reactor powder having the further lower DR_{max} of ∼6, independent of drawing techniques.

Initial Morphologies. To choose the possible T_p below oxidation, DSC measurements of reactor powder were made under several conditions. An exotherm around 190 °C, due to sample oxidation, was clearly observed on a heating scan for reactor powder in air. Under a nitrogen gas flow, such an exotherm did not appear up to, at least, 260 °C. To reduce oxidation, 0.5 wt % antioxidant was added to the powder. DSC thermograms of the powder, which contained antioxidant, showed no exotherm up to 260 °C, even in air. The molding of films were made in air; thus, a T_p range of 160−230 °C was chosen for the preparation of a series

Table 1. DSC Characteristics and Densities of MGC Films from Reactor Powders Having Various Thermal Histories

prior-melt temp (°C), time (min)	T_m (°C)[a]	ΔH_f (J/g)[a]	% cryst	density (g/cm^3)	% cryst
reactor powder	140.5	195	67.2		
160, 5	133.8	157	54.1	0.9363	54.5
180, 5	134.6	155	53.4	0.9363	54.5
200, 5	134.2	149	51.4	0.9361	54.4
200, 35	134.2	150	51.7	0.9340	52.9
200, 300[b]	134.4	152	52.4	0.9364	54.6
200, 300[c]	134.4	148	51.0	0.9336	52.6
200, 6000	134.5	149	51.4	0.9331	52.2
230, 5	134.5	155	53.4	0.9368	54.9

[a] Measured at 3 °C/min. in N_2 gas. [b] As prepared (not extracted). [c] Silicone extracted with acetone in a soxhlet.

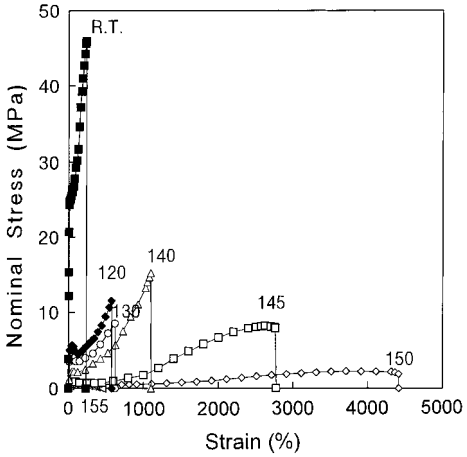

Figure 1. Nominal stress/strain curves recorded at the indicated temperatures (T_d in °C) for MGC films compression molded at 180 °C (T_p) for 5 min from reactor powder.

of MGC films. No change in infrared spectroscopy was observed for the entire T_p series of MGC films prepared in this work.

Table 1 shows the DSC characteristics, including $T_{m,peak}$ and ΔH_f, and crystallinities (in wt %) calculated from both ΔH_f and the measured densities for MGC films compression molded at different T_p's of 160−230 °C. As seen in Table 1, crystallinity values determined from these different evaluation methods are in good agreement. For some MGC films compressed at 200 °C, subsequent melt−annealing was carried out in a silicone oil bath at T_a = 200 °C for 30 min to 24 h. Independent of silicone treatment, molding temperature, or following annealing conditions, the $T_{m,peak}$ and crystallinity show constant values of 134.5−135.0 °C and 52.5−54.5%, respectively. No significant differences in the initial morphology was observed for the DSC characteristics and densities of this series of MGC films melted previously under different conditions. Only the initial reactor powder has different characteristics.

Effect of T_d on Draw Behavior. Figure 1 compares the stress/strain curves of MGC films, drawn at T_d = RT−155 °C and an initial strain rate of 5 min^{-1}. Preparation of the initial MGC film from reactor powder was made at T_p = 180 °C for 5 min. At T_d = RT, the draw stress increased rapidly in a low-strain region (<10%), and the sample broke around a low DR = 3. No necking was observed, and a uniform deformation occurred.

The tensile-drawing behavior at 120−150 °C could be separated into two T_d groups, 120−130 and 140−150 °C. For the former, the stress increased quickly up to ∼5 MPa at low strain, <10%, and further gradually increased with increasing strain (see Figure 1). The samples broke around DR = 6 at T_d's of 120 and 130 °C. The nominal stresses for tensile drawing decreased with increasing T_d. In the higher T_d range, the DR_{max} increased with increasing T_d from DR_{max} = ∼10 at T_d = 140 °C to 45−50 at 150 °C. Thus, the strain increased, and the stress at break significantly decreased with increasing T_d. A combination of higher DR_{max} and lower values of final draw stress exhibit a gentler slope of the curve at higher T_d. Such a lower stress during draw in this T_d region corresponds to a lower viscosity of UHMWPE at higher temperatures. These stress/strain curves at T_d = 145 and 150 °C exhibited an apparent yield just before sample break, as detected with Figure 3. At T_d = 155 °C and above, drawability dropped markedly. When the draw stresses were compared at the same strain, they also decreased with increasing T_d; thus, the deformation proceeded with the lower energy at the higher T_d. However, the total deformation energy up to the sample breaking, evaluated from the area under the curves, also depended on the maximum strain (DR_{max}) at each T_d. The total energy more than doubled when T_d was increased from 120 to 145 °C. The area under the curve at T_d = 145 °C exceeded that at T_d = RT. At 150 °C and above, the total energy abruptly dropped.

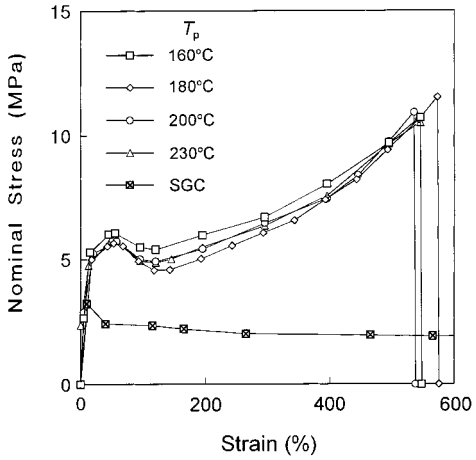

Figure 2. Nominal stress/strain curves recorded at T_d = 120 °C (below sample T_m) for MGC films compression molded at various T_p's for 5 min. The draw curve of a SGC mat recorded at T_d = 120 °C is also included.

Finally, the UHMWPE film was found not to be solid-state drawn well, DR 6−5, but it could be ultradrawn after rapid melting. For MGC film prepared at T_p = 180 °C, the optimum T_d was 150 °C, where the sample could be drawn up to a DR_{max} of 45−50. The resultant maximum achieved tensile modulus and strength were 55 and 0.95 GPa, respectively.

Effect of T_p and Prior Annealing on Drawing from Melt. A T_p effect on drawing behavior in both solid and molten state was examined for a MGC series prepared from reactor powders at various T_p's and compared to that for draw of SGC mats. Figure 2 shows the stress/strain curves observed at T_d = 120 °C for the MGC series prepared at T_p = 160−230 °C. Tensile drawing was made at an initial strain rate of 5 min^{-1}. For comparison, data are shown for draw of SGC mats at 120 °C, which could be ultradrawn up to a DR_{max} of ∼100. For MGC films, the draw stress increased rapidly

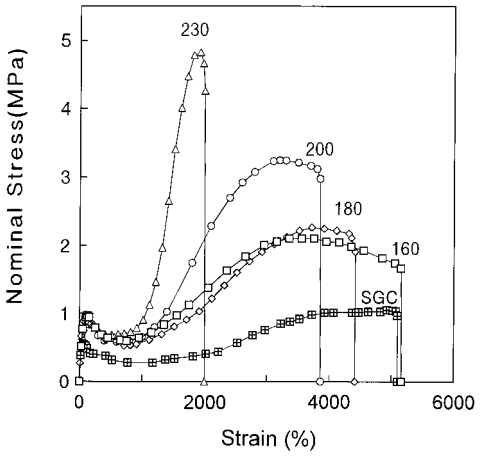

Figure 3. Nominal stress/strain curves recorded at $T_d = 150$ °C (above sample T_m) for MGC films compression molded at various T_p's. The draw curve of an SGC mat recorded at $T_d = 150$ °C is also included. The numbers on the curved indicate T_p in °C.

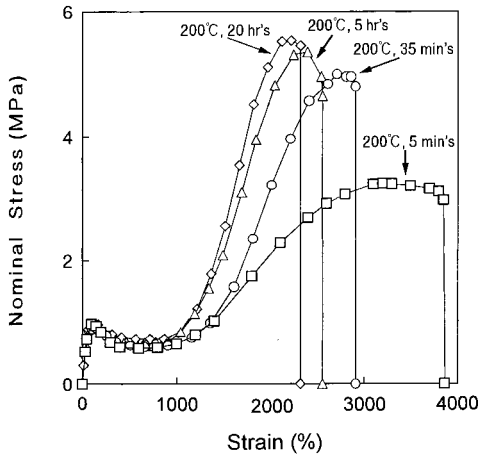

Figure 4. Effect of melt−annealing time (t_a) on nominal stress/strain curves recorded at $T_d = 150$ °C for MGC films compression molded at $T_p = 200$ °C. Prior melt annealing was made at $T_a = 200$ °C in a silicone oil bath for different times before drawing.

below a low strain of ∼20%, followed by a neck deformation around 60%. Above a DR of 2−3, strain hardening became significant, and the sample broke around a DR_{max} of 6.5. These stress/strain characteristics of MGC films were identical and independent of T_p. Indeed, Lemstra et al.[21] have reported that the same stress/strain curve was observed in the solid state for UHMWPE samples annealed above T_m for a short period (∼30 s) and independent of prior sample preparation. Our results of no effect of T_p on the stress/strain curves for MGC films are consistent with their previous data. Indeed, the DSC characteristics and measured densities show constant values, independent of T_p (see Table 1).

According to the Smith's entanglement concept,[7] drawability in the solid state is determined by the entanglement density in the sample. Thus, the same DR_{max} for the MGC series prepared at different T_p's suggest the existence of the same entanglement density for the MGC series. This estimation, combined with the data in Table 1, implies that the initial morphology is not distinguishable. In other words, seemingly, the different entanglement formation could not be prepared by changing T_p. The draw stress for SGC mats was much lower than those of MGC films (see Figure 2). This difference in the stress/strain curves between MGC films and SGC mats could primarily be attributed to the higher and apparently uniform entanglement density of the MGC films.

In contrast, it was found here that, on drawing from a "molten state", the effect of T_p on stress/strain curves could be clearly observed. Figure 3 compares the stress/strain curves recorded at $T_d = 150$ °C for the same series of MGC films as that in Figure 2. The data for drawing of a melt SGC mat is also included. These stress/strain curves differ markedly from those recorded at $T_d = 120$ °C, as shown in Figure 2. Higher DR_{max} and lower draw stress data were obtained for the drawing from "melt" than those in the solid state. On these stress/strain curves, two peaks were clearly observed for each sample. When draw was started, the draw stress increased rapidly with strain. At a strain of ∼200%, the first peak was observed, likely corresponding to the onset of orientation. Subsequently, the stress decreased gradually, followed by reaching to a constant value of ∼0.7 MPa around a DR of ∼10. In this strain region, this curve shape is similar for different T_p samples, except for the SGC mat. Above a DR of ∼10, draw stress increased again. In this strain region, the slope of the stress/strain curve becomes steeper with increasing T_p. This means that a larger deformation energy was required on drawing above a certain strain around 10 for the films prepared at higher T_p's. As shown below, strain-induced, oriented crystallization occurred above a DR of ∼10 even at $T_d = 150$ °C, which was evaluated from DSC and X-ray measurements. The increase in the draw stress above a DR ≈ 10 is attributable to this morphological change. After such a rapid stress increase, the draw stress reaches an apparent yield. This yield is related to the reducing sample cross-sectional area at the higher DR. The DR_{max} decreased, and the stress at break increased with increasing T_p, as shown in Figure 3. The draw stress of the SGC mat, which had a low initial entanglement density, was remarkably lower than those of MGC films even at a melt temperature.

Melt time effects on drawing from a molten state was also examined. MGC films were further annealed above the T_m for various time (t_a) before draw. Figure 4 compares the stress/strain curves recorded at $T_d = 150$ °C for the MGC films prepared by compression molding at $T_p = 200$ °C, followed by melt−annealing at 200 °C for $t_a = 5$ min to 20 h in a silicone oil bath. The T_m, ΔH_f, and measured densities of these samples were constant, independent of prior-melt−annealing conditions (see Table 1). Even when t_a was extended, the same stress/strain curve was recorded below a strain of ∼10, consistent with the draw from melt for the MGC films prepared at different T_p's (see Figure 3). In an earlier stage of drawing from the melts, the stress/strain behavior is affected by neither the prior-melted temperature nor time. Below a DR of ∼10, the strain-induced crystallization has not occurred, as will be discussed later on the basis of WAXD and DSC data (Figures 6−9). Namely, the draw stress could be determined only by the amorphous fluidity. Above a DR of ∼10, the draw stress increased rapidly for each of the samples where the strain-induced crystallization occurred. In this strain region, the slope of the stress/strain curve becomes steeper with increasing t_a (see Figure 4). A higher draw stress was observed on the stress/strain curve for the MGC films melt−annealed

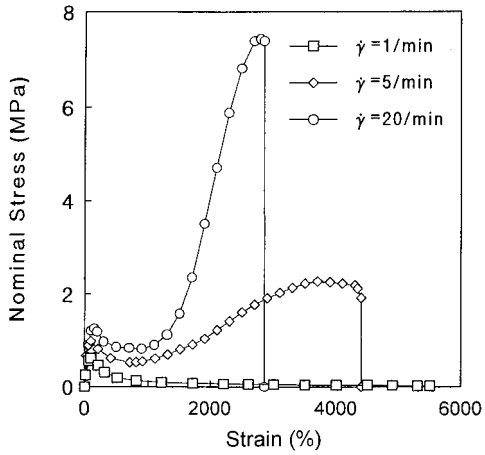

Figure 5. Nominal stress/strain curves recorded at the initial strain rates of 1−20 min^{-1} for MGC films compression molded at T_p of 180 °C. Draw was made at 150 °C (above sample T_m).

for longer t_a's. Correspondingly, the maximum achievable DR_{max} decreased with increasing t_a. Especially for shorter t_a's, these trends were significant. The t_a effects on the stress/strain curves are similar to those of T_p for drawing from melt, as shown in Figure 3.

Effect of Draw Rate on Tensile Stress/Strain Behavior of Melt. Draw from the melt was also markedly affected by draw rate, comparable to the solid-state draw of less-entangled SGC.[5] Figure 5 compares the stress/strain curves recorded at constant cross-head speeds giving different initial strain rates, $\dot{\gamma}$, for drawing at a T_d = 150 °C. The sample was prepared by compression molding at T_p = 180 °C. At $\dot{\gamma}$ = 1 min^{-1}, draw could be achieved up to a DR around 55. However, its stress/strain curve shows a continuous decrease in stress even at the higher extension. Correspondingly, the WAXD pattern of the resultant sample drawn up to a DR_{max} of 60 exhibited the reflection arcs, indicating low orientation of the crystalline chains. These show a poor efficiency of draw at the lower $\dot{\gamma}$. Chain slippage had readily occurred. In contrast, at the higher $\dot{\gamma}$ of 20 min^{-1}, the plateau region up to a strain around 10 shows a higher stress level and a more rapid increase in stress beyond this plateau strain. The sample could be drawn up to a DR_{max} of 30 at such a higher $\dot{\gamma}$, compared to a DR_{max} = 45 obtained at a lower $\dot{\gamma}$ of 5 min^{-1}. This indicates that the chains can more effectively transmit the draw stress with a more rapid melt-draw.

Crystallinity Development during Melt Draw. It is known that orientation-induced crystallization can occur during draw.[21,22,24−26] In this work, the effect of prior-melt conditions on such a structural change during drawing above the static T_m was examined by X-ray and DSC measurements.

Figure 6 shows WAXD patterns obtained at RT for an undrawn MGC film prepared at T_p = 180 °C and its DR series prepared at T_d = 150 °C. The crystal form was orthorhombic in each sample. The pattern of an undrawn MGC film exhibited uniform rings of the (110) and (200) reflections. At a DR of 12, the (110) reflection consists of a circular spot overlapped with a fairly broad arc centered on the equator. In contrast, the (200) appears as a circular spot. This indicates that the *a*-axis of all crystals is well oriented perpendicular to the draw direction. However, although the *b*-axis of some crystals shows a high chain orientation, that of other crystals has a lower orientation to the fiber axis, which suggests the coexistence of two types of crystals having different chain orientation. Such a structure at a low DR is likely related to the "shish-kebab" morphology often found in

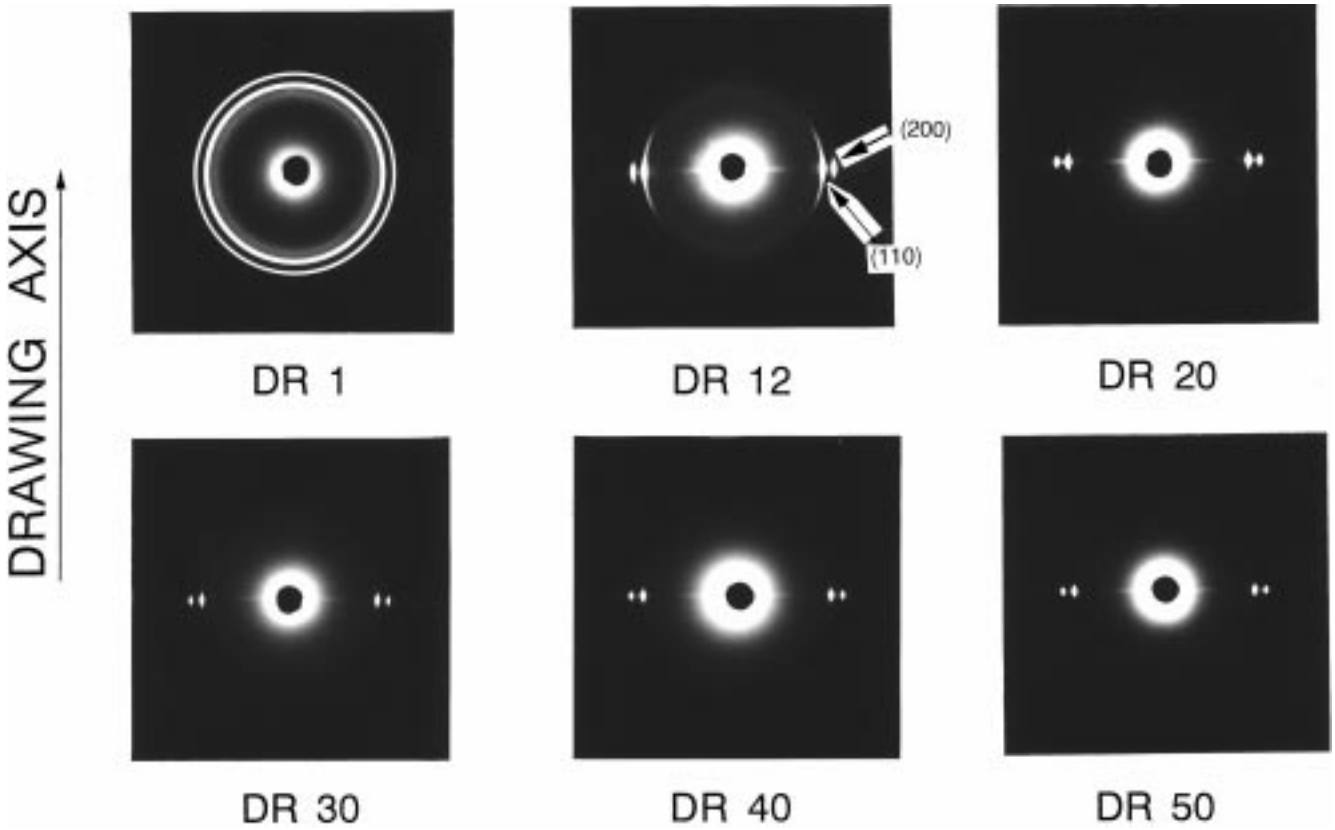

Figure 6. WAXD patterns of an undrawn sample and a DR series of samples drawn at T_d = 150 °C from an MGC film compression molded at T_d = 180 °C.

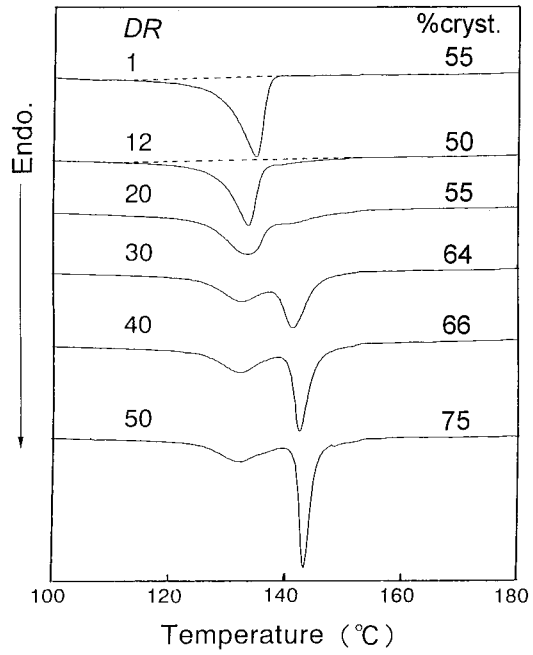

Figure 7. Changes in DSC melting thermograms on drawing for a MGC film molded at T_p = 180 °C. Draw was made at 150 °C. Crystallinity values, calculated from the sample ΔH_f, were also included.

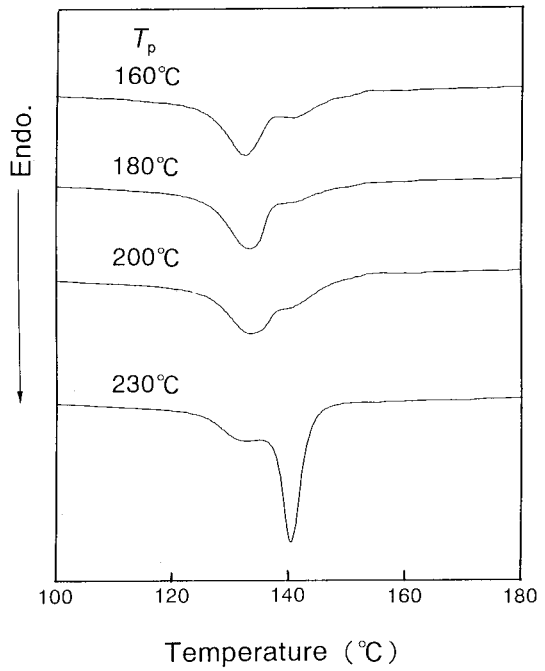

Figure 8. DSC melting thermograms for the drawn samples with a constant DR of 20, prepared at T_d = 150 °C from MGC films molded at different T_p's, as indicated.

melt-drawn samples.[31] Only spots were observed at a DR of 20. This shows that the orientation-crystallization occurs rapidly above DR of ~12 on melt drawing at 150 °C. With increasing DR, the spot reflection becomes sharper, suggesting the more oriented crystallization from the melt.

Figure 7 compares the DSC thermograms observed at a *H. R.* of 3 °C/min for the same DR series as shown by WAXD results in Figure 6. The melting endotherm of an undrawn MGC film (DR = 1) exhibited a single peak around 135 °C, corresponding to the melting of lamellae crystallized on slow cooling after compression molding at T_p = 180 °C. At a DR of 12, the $T_{m,peak}$ shifted lower to ~132 °C. This T_m decrease suggests that folded crystals, formed during cooling to RT after draw at T_d = 150 °C, had a smaller lamellae thickness. The total crystallinity, calculated from the sample ΔH_f, also decreased from ~55% for an undrawn film to ~50% for a DR12 film. A slight tail was also observable on the high-temperature side of the main melting peak. With increasing DR, this higher-temperature tail gradually grew into an apparent endothermic peak.

WAXD patterns showed the coexistence of highly ordered and less oriented crystals for the lower DR samples, as shown in Figure 6. It is known that the chain-extended crystals exhibit higher T_m than that of the folded lamellae. Thus, these high-temperature endotherms suggest the melting of the highly chain-extended and oriented crystals formed during the melt draw. At a DR of 30, the thermograms clearly exhibited double melting peaks at 132 and 142 °C, and the high-temperature peak became the major peak. The crystallinity, calculated from ΔH_f, increased from ~55% for a DR20 film to ~64% for a DR 30 film. These crystallinity values are in agreement with those calculated from the measured density. Such a rapid crystallization with a high chain orientation around a DR of 20−30 corresponds to the significant increase of draw stress in this strain region, as shown in Figure 3. At higher DRs, this peak developed more abruptly, corresponding to the further enhancement of chain orientation, revealed by the WAXD patterns (see Figure 6). It should be noted that the peak position of the low-temperature side peak was always located around 132 °C, below the initial T_m of 135 °C and independent of DR. This fact, combined with the high chain orientation for the highly drawn products (Figure 6), suggests that the crystals showing the lower T_m occurred on cooling from T_d = 150 °C at a constant sample length (20−50 cm). In contrast, the position of higher-temperature peak shifted slightly higher with increasing DR. Thus, the longitudinal size of the highly chain-extended and oriented crystals, as well as their amount, apparently increased by more deformation on melt draw.

These results indicate that flow-induced oriented crystallization can occur on draw from the melt, as reported[31], depending on draw ratio, temperature, and rate. Sample crystallinity increased from 55% up to 75% for the DR series, as shown in Figure 7. The stress/strain curves recorded at a given draw rate depended on the prior T_p and t_a, as shown by tensile draw tests in Figures 3 and 4. The effect of such different prior melt conditions on orientation-induced crystallization during drawing from the melt was also evaluated from DSC melting characteristics of the drawn samples. Figures 8 and 9 compare the T_p effect on DSC thermograms at DRs of 20 and 40, respectively. The samples were obtained on drawing at T_d = 150 °C. DSC scans were made at a *H. R.* of 3 °C/min.

At a DR of 20 in Figure 8, the thermograms were similar among the samples drawn from the MGC films molded at T_p = 160−200 °C. The crystallinity, calculated from the sample ΔH_f, increased slightly from ~55% to ~59% with increasing T_p. The lower-temperature DSC peak was the major peak for these samples. A higher-temperature peak at a given DR, corresponding to the melting of the chain-extended crystals, was much larger than those prepared from the films molded at lower T_p's. On draw of this highest T_p sample, the higher-temperature peak became the major peak and the low-tem-

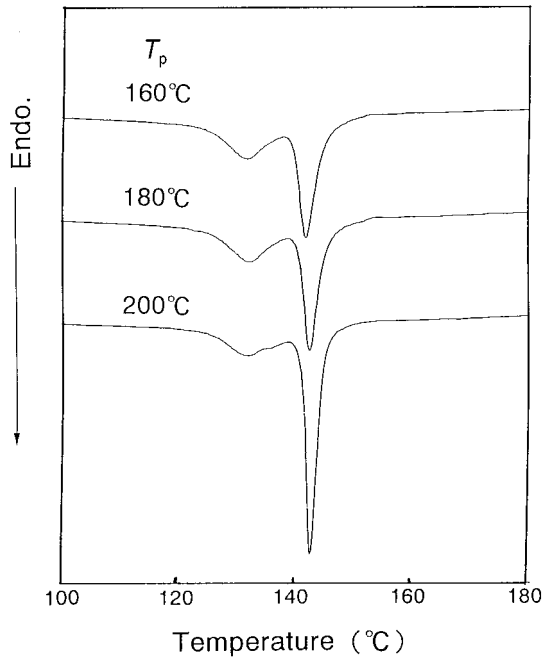

Figure 9. DSC melting thermograms for the drawn samples with a constant DR of 40, prepared at $T_d = 150$ °C from MGC films molded at different T_p's, as indicated.

perature peak decreased into a slight tail at a DR of 20. This indicates the formation of a larger amount of chain-extended and oriented crystals for the samples drawn from the films prior-melted at higher T_p's, even at the same DR. The position of lower-temperature peak was ~132 °C, independent of T_p and DR (Figure 7). In contrast, that of the higher one increased with increasing DR, but independent of T_p at the same DR.

The area components of low- and high-temperature DSC peaks are compared for DR of 20 and 40 in Figures 8 and 9, respectively. The high-temperature peak grows over that of the low-temperature peak for all T_p samples. Even for lower T_p samples, the higher-temperature peak became the major peak at a DR of 40. Figure 9 shows comparable thermograms for the samples drawn from MGC films molded at 160 and 180 °C. A comparable crystallinity of ~66%, calculated from ΔH_f, was observed for these two samples. However, the sample prepared from the film molded at a higher $T_p = 200$ °C exhibited a sharper high-temperature peak at the same DR of 40. An abrupt increase of crystallinity up to ~71% was observed for this $T_p = 200$ °C sample.

Efficiency of Draw by Thermal Shrinkage. As shown in Figures 1 and 4, MGC films could be drawn up to $DR_{max} \approx 50$. To evaluate chain extension, the elastic recovery was measured by thermal shrinkage tests. Figure 10 shows recovery percentages for various DR samples, previously compressed at different T_p's. Optimum drawing was obtained at a $T_d = 150$ °C and at an initial strain rate of 5 min^{-1}. The samples drawn from the films prepared at $T_p = 160-200$ °C exhibited low recovery values of 83−88% in a lower DR region of 12−15. Above a DR of ~20, recovery reached a constant higher fraction of ~90%, independent of DR and prior T_p. This means that the molecules are highly extended and oriented within the drawn products.

These elastic recovery percentages are slightly lower than those obtained for solid-state drawing of SGC mats. However, they indicated that the molecular chains within the strain-induced crystallized component, showing a high T_m of 143 °C, were highly oriented and chain-extended during drawing from melt. Such higher efficiency of draw for the higher T_p films may be explained by "effective" entanglements formed at a higher T_p, which could transmit the applied stress even on melt draw.

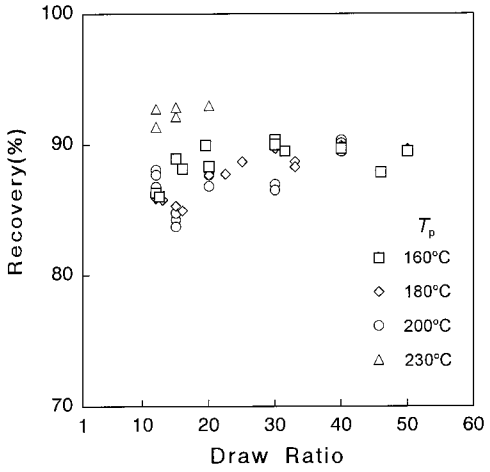

Figure 10. Thermal elastic recovery as a function of DR for samples drawn at 150 °C from MGC films compression molded at different T_p's. Draw was made at the initial strain rate of 5 min^{-1}.

Discussion

Effect of Prior-Melt−Annealing Conditions on Drawability. Combination of the "melt" conditions on the stress/strain curves both in the solid-state and molten-state leads to the following ideas. On solid-state drawing, the same resistance to draw was found, even if the samples had different prior-melt histories (see Figure 2). However, the stress/strain curves on drawing above the static T_m were significantly affected by the prior-melt conditions (Figures 3 and 4). These results suggest that the entanglements effective on draw from the melt increased sensitively with increasing prior melt−annealing temperature and time, because of the development of deep entanglements by the chain diffusion. This is consistent with the lower draw stress for drawing from the melt of the initially less-entangled SGC. By melt treatment, we have apparently generated different levels of entanglement. At higher T_p or for longer t_a, semipermanent entanglements seem to be formed. In contrast, at lower T_p or for shorter t_a, the entanglements developed would seem to be transient and easily disentangled during melt draw. Both levels of entanglements effectively reduce solid-state draw; thus, DR_{max} was independent of the prior thermal histories (see Figure 2). In Figure 4, the stress/strain curves were comparable for the samples annealed for the longer t_a's (for example, $t_a = 5$ vs 20 h).

Origin of Low-Temperature Endotherms for the Samples Drawn from Melts. The double melting endotherms were generally observed for samples drawn from the melts. Even at a high DR_{max} of 50, the lower-temperature DSC peak still appears (see Figure 7). In contrast, for drawing of SGC in a solid state, only the higher melting peak was observed.[9] Further, the higher temperature peak showed a significant superheating as was observed for melting of ultradrawn solution-crystallized samples. On drawing from melts, the "deeply" entangled regions concentrate during orientation crystallization.

Oriented Crystallization Evaluated from DSC Measurements. The DSC curves in Figures 8 and 9 allow an evaluation of crystallization as a function of DR. The high-temperature peak measures the amount of crystals formed by strain-induced crystallization during draw. The DSC thermograms for higher DR40 and lower DR20 films suggest that the crystallization rate, as a function of DR, is higher for drawing from melt of the MGC films prepared at a higher T_p. The higher draw stress, possibly transmitted by "deep" entanglements formed at a higher T_p, induces this higher crystallization rate on draw even at the same T_d of 150 °C. This trend is consistent with the rapid increase of draw stress above DR ≈ 12 for the higher T_p samples, as seen in Figure 3. These different crystallization rates on draw from melt, reflecting the prior thermal history of the samples, also suggest the inducement of two levels of entanglements (deep and shallow) formed at different T_p's.

Relaxation Influence on Effective Entanglement Depth. The idea of the coexistence of shallow and deep entanglements in melt is consistent with the observed effect of draw rate on the stress/strain behavior (see Figure 5). The relationship between draw stress and draw rate obtained at low and high $\dot{\gamma}$'s is quite similar to that observed for T_d and t_a effects on drawing behavior above the T_m, as shown in Figures 3 and 4. Thus, it could be concluded that these $\dot{\gamma}$ effects suggest that the entanglement depth depends on the time allowed for the UHMWPE chain relaxation during draw in the molten state. A slow draw rate brings an ease of amorphous chain relaxation, which is necessary for disentanglement. At the higher $\dot{\gamma}$, an entanglement responds to more efficient force transfer. These entanglement depth influences on the series of stress/strain behaviors, examined in this work, were observable only for UHMWPE, whereas the drawing from the conventional MWPE melt is limited because of its low viscosity.

Entanglement Formation Evaluated by Drawing or from Viscoelastic Measurements. Bastiaansen et al.[20] examined the memory effect of polyethylene melts prepared from solution- and melt-crystallized morphologies by viscoelastic measurements made on the melts at 160 °C. They concluded that the entanglements formed rapidly by the segmental (not total molecular) mobility, estimated from the similar viscoelastic response for both of the prior morphologies. It has been reported that the memory effect of prior crystallization history of samples was lost after heating into melts even for a short time (30 s).[20] These gave us the expectation that the prior-melt conditions for preparation of MGC films does not affect the nature of the amorphous melts. Nevertheless, on drawing from the melt, the difference in induced entanglements could be observed. Deep "semipermanent entanglements" that interrupt high draw require a higher prior-melt−annealed temperature or a longer time to develop and are assumed to not be disentangled even in high-strain draw.

On the Possible Meaning of Similar Stress/Strain Curve at Low Strain. Figures 3 and 4 show an equivalent curve shape at low strain, independent of prior-melt conditions. This indicates that fluidity of the melts reaches a semiequilibrium melt at an earlier stage of draw in terms of chain relaxation. In addition, reported viscoelastic data in the melts is consistent with our stress/strain behavior in a low-strain region.[20] Both phenomena might be explainable by the same concept. It should be emphasized that the rapid increase of draw stress was detected only at higher strain (>∼1000%), where the segment between entanglements was extended and oriented, leading to the oriented crystallization. These imply that viscoelastic measurements may not an effective method to estimate a dependence of prior-melt−annealing on the entanglement state. These effects of prior thermal histories on drawability and draw stress appear to exhibit different entanglement roles on melt drawing.

Memory Effect of Reactor Powder Morphology on Drawing from Melt. The likely developments of entanglements in the melts suggest an unique morphology of UHMWPE reactor powder. The initial less entangled state of reactor powder enables further formation of entanglements on melt−annealing. At a lower T_p, the shallow "transient entanglements" did not restrict melt draw. This means that a relatively less-entangled state could be maintained, even in a melt for a short time. This memory effect of reactor powder morphology apparently allowed the high-melt draw up to a DR_{max} of ∼50. Lower temperature drawability was independent of melt−annealing conditions (see Figure 2). The total entanglements effective on a solid-state draw were both high and similar, with DR ≈ 6.

Conclusions

MGC films prepared from UHMWPE reactor powders at different molding temperatures of 160−230 °C could be drawn from a molten state up to a high DR_{max} of ∼50, depending on draw conditions. Any significant differences in the initial morphology could not be observed from the DSC characteristics (T_m ≈ 135 °C and ΔH_f ∼ 150 J/g) and densities (∼0.935 g/cm^3) of these MGC films. However, the drawability and resultant physical properties were significantly affected by prior molding conditions. Equivalent stress/strain curves were recorded at low extension DR < 10, independent of the prior-melt temperature of MGC films. Even when the prior-melt−annealed time was extended beyond 5 min, equivalent stress/strain curves were found at low strain.

The results of DSC and WAXD measurements clarify that the strain-induced crystallization occurred above a strain of ∼DR10 on draw at 150 °C. At such high strain, the stress/strain curves on drawing from melt were significantly affected by the prior-melt conditions. Deformation proceeded smoothly for the films prepared at lower melt temperatures or shorter times. These results suggested that the entanglements effective on draw increased with increasing prior-melt−annealing temperature and time. The coexistence of two kinds of induced entanglements in the melts was observable. At higher melt temperature or for longer annealing time, deep semipermanent entanglements seemed to be formed, which could transmit draw stress even in melt flow. In contrast, at lower melt temperature, entanglements formed are considered shallow and transient, and disentangled during orientation−crystallization from the melts. The effect of draw rate on stress/strain behavior shows that the efficiency of such entanglement changes, depending on the chain relaxation level at a given deformation condition from the melt. The DSC data of samples drawn from melt exhibited that the higher draw stress, effectively transmitted by deep entanglements, induces a rapid crystallization during draw. However, the total entanglements, evaluated from

drawability in the solid state, are independent of prior-melt conditions. The maximum achievable tensile modulus and strength obtained for the products drawn from melt were 55 and 0.95 GPa, respectively, in this work.

Acknowledgment. The authors thank Prof. M. Ito (Department of Chemistry, Science University of Tokyo) for helpful discussions and the use of his instruments. Drs. A. Waddon in UMass (University of Massachusetts) and S. Ottani in University of Bologna in Italy also gave valuable suggestions on this work. For accomplishment of these studies, appreciation is expressed for the utilization of the NSF MRSEC Grant at UMass.

References and Notes

(1) Zwijnenburg, A.; Pennings, A. J. *Colloid Polym. Sci.* **1976**, *254*, 868.
(2) Smith, P.; Lemstra, P. J.; Pijpers, J. P. L.; Keil, A. M. *Colloid Polym. Sci.* **1981**, *259*, 1070.
(3) Lemstra, P. J.; Smith, P. *J. Mater. Sci.* **1980**, *15*, 505.
(4) Kanamoto, T.; Tsuruta, A.; Tanaka, K.; Takeda, M.; Porter, R. S. *Polym. J.* **1983**, *15*, 327.
(5) Kanamoto, T.; Tsuruta, A.; Tanaka, K.; Takeda, M.; Porter, R. S. *Macromolecules* **1988**, *21*, 470.
(6) Griswold, P. D.; Zachariades, A. E.; Porter, R. S. *Polym. Eng. Sci.* **1978**, *18*, 861.
(7) Smith, P.; Lemstra, P. J.; Booij, H. C. *J. Polym. Sci., Polym. Phys. Ed.* **1981**, *19*, 877.
(8) Sakurada, I.; Ito, T.; Nakamae, K. *J. Polym. Sci., Part C* **1966**, *15*, 75.
(9) Kanamoto, T.; Ohama, T.; Tanaka, K.; Takeda, M.; Porter, R. S. *Polymer* **1987**, *28*, 1517.
(10) Okuyama, H.; Kanamoto, T.; Porter, R. S. *J. Mater. Sci.* **1994,** *29*, 6485.
(11) Uehara, H.; Ito, S.; Okuyama, H.; Kanamoto, T.; Porter, R. S. *Rep. Prog. Polym. Phys. Jpn.* **1995**, *38*, 331.
(12) Smith, P.; Chanzy, H. D.; Rotzinger, B. P. *Polym. Commun.* **1985**, *26*, 258.
(13) Rotzinger, B. P.; Chanzy, H. D.; Smith, P. *Polymer* **1991**, *30*, 1814.
(14) Wang, L. H.; Ottani, S.; Porter, R. S. *Polymer* **1991**, *32*, 1776.
(15) Uehara, H.; Nakae, M.; Kanamoto, T.; Ohtu, O.; Sano, A.; Matsuura, K. *Polymer* **1998**, *39*, 6127.
(16) Rahl, F. J.; Evanco, M. A.; Fredericks, R. J.; Reimschuessel, A. C. *J. Polym. Sci., Part A-2* **1972**, *10*, 1337.
(17) Yamaguchi, S. *Koubunshi Ronbunshu* **1982**, *39*, 493.
(18) Folda, T.; Hoffman, H.; Chanzy, D. H.; Smith, P. *Nature* **1988**, *333*, No. 6168, 55.
(19) Waddon, A. J.; Keller, A. *J. Polym. Sci., Polym. Phys. Ed.* **1990**, *28*, 1063.
(20) Bastiaansen, C. W. M.; Meyer, H. E. H.; Lemstra, P. J. *Polymer* **1990**, *31*, 1435.
(21) Lemstra, P. J.; van Aerle, N. A. J. M.; Bastiaansen, C. W. M. *Polym. J.* **1987**, *19*, 85.
(22) Uehara, H.; Kanamoto, T.; Murakami, S.; Kawaguchi, A. *Macromolecules* **1996**, *29*, 1540.
(23) Porter, R. S.; Johnson, J. F. *Chem. Rev.* **1966**, *66*, 1.
(24) Ferry, J. D. *Viscoelastic Properties of Polymers*, 2nd ed.; Wiley: New York, 1970.
(25) Graessley, W. W. *Adv. Polym. Sci.* **1974**, *16*, Ch. 7.
(26) Ottani, S.; Porter, R. S. *Mokromol. Chem. Rapid. Commun.* **1995**, *16*, 813.
(27) Folland, R.; Charlesby, A. *Eur. Polym. J.* **1979**, *15*, 953.
(28) Wunderlich, B.; Cormier, C. M. *J. Polym. Sci., Polym. Part A-2* **1967**, *5*, 987.
(29) Kaito, A.; Nakayama, K.; Kanetsuna, H. *Polym. J.* **1982**, *14*, 757.
(30) Van Aerle, N. A. J. M.; Lemstra, P. J. *Makromol. Chem.* **1988**, *189*, 1253.
(31) Bashir, Z.; Keller, A. *Colloid Polym. Sci.* **1989**, *267*, 116.

MA981491Z